

Crashworthiness optimization of foam-filled beams with dissimilar materials under lateral impact

Yong Sun, Shu Yang*, Chang Qi*

Dalian University of Technology, Dalian, 116024

Email: g21422003@mail.dlut.edu.cn, yangshu@dlut.edu.cn, qichang@dlut.edu.cn

Abstract: To this end last few decades have witnessed an increasing interest on dissimilar materials vehicle bodies, which includes high strength steel and aluminum alloy. This paper aims to explore the lateral crashworthiness of foam filled beams made of dissimilar materials in both passenger and pedestrian protection. After validating FE models of empty beam and aluminum foam, the radial basis function (RBF) metamodels are constructed to predict the crashworthiness criteria for variations in load positions. The Pareto fronts are identified for bi-objective (F_{ip} , SEA) and tri-objective (F_{ip} , SEA , Mb) optimization under both specific load position and the cases including multiple load positions, using the multi-objective particle swarm optimization (MOPSO). It is found that the optimal designs were generally different with different load positions. Taking load position uncertainties into consideration, the results of tri-objective optimization also revealed that weighting factors have some influence on the disproportionate between SEA^P and Mb^P . The results demonstrate foam-filled beams with dissimilar materials can be an efficient energy absorber.

Keywords: foam-filled; dissimilar materials; lateral impact; load position uncertainty; multi-objective optimization

1 Introduction

Under the requirement for emission reduction and environment protection, automotive lightweight in passive safety design has received considerable academic attention. To effectively enhance vehicle crashworthiness, as well as lightweight, thin-walled structures have been commonly employed as energy absorbers in crash applications for protection both passengers and pedestrians.

In recent years, research attention on materials has been shifted from conventional materials to advanced lightweight materials, such as advanced aluminum alloy because of its commendable energy absorb abilities and lightweight characteristic [1-3]. Despite the advantages of weight reduction, aluminum structures are usually restrained by higher cost and poorer impact intrusion compared with steel counterparts. To fully utilize advantages of steel and aluminum alloy, dissimilar materials structures were proposed. In this regard, Zhou et al. [4] proposed an S-shaped front rail made of steel-aluminum hybrid materials to reduce the peak impact force and the total weight when adopted in vehicle's frontal frame. Gedikli [5, 6] and Meric [7] conducted an investigation on aluminum-steel empty and foam-filled tailor-welded tubular structures under axial impact, and material types together with tube configurations were found to have significant effect on axial crashworthiness. Additionally, Wang et al. [8] revealed that tapered tailor welded tubes made of dissimilar materials outperformed its homogeneous counterparts for stable deformation and energy absorption when oblique impact is inevitable. Up to date, hybrid materials structures are believed to be a potential option for energy absorption components.

However, besides focus on wall materials, filler materials, such as honeycombs [9], polyethylene foams [10] and metal foams [11], have also been intensively studied for decades, since those fillers are commonly characterized by increasing energy absorption capability without improving volume and too much weight. Automotive industry applied aluminum foam with aluminum alloy to make the vehicle body as strength as steel body.

The abovementioned studies mostly focused on the crushing design of thin-walled tubes for pure axial or oblique impact, while bending situations occurred more frequently on vehicle bodies in accidents, such as the bumper beams, the B-pillars and so on. Therefore, this paper contributed to crashworthiness of foam-filled beams with dissimilar materials under lateral loads.

For further research on crashworthiness of foam-filled thin-walled structures under transverse impact, extensive attention has been drawn in recent years on the structural optimization techniques. In contrast to the plentiful studies on axial loads, a limited number of studies have reported on bending optimization. Sun et al. [12] applied multi-objective optimization to further compare the lateral crashworthiness between the functionally graded thickness tubes and the uniform thickness tubes. However, only single load condition was assumed in these optimizations, complicated load

conditions may not be include. To the best of the author's knowledge, there have been no published studies addressing the crashworthiness optimization of foam-filled beams with dissimilar materials subject to different load positions.

In the previous study, a new type of double-hat thin-walled beam composed of an aluminum alloy upper hat and a steel lower hat riveted were proposed [13]. To further enhance energy absorb capability, the bending behavior of foam-filled beams with dissimilar materials will be explored in this paper. The aim of this study was to address the crashworthiness design for foam-filled beams under bending. To optimize the crashworthiness criterions, the multi-optimization for foam-filled beams with dissimilar materials with dissimilar materials on multiple load positions are formulated, providing a basis for further automobile body design.

2 Method and Material

2.1 Structural crashworthiness indicators

Several different criteria are commonly used to evaluate crashworthiness of thin-walled beams with dissimilar materials under lateral loading, such as energy absorption (EA), specific energy absorption (SEA), and initial peak force (F_{ip}). Among those indices, SEA is generally applied to indicate the crashworthiness of structures considering the energy absorption capacity and weights systematically. SEA denotes the energy absorption per unit mass of the profiles, which can be expressed as

$$SEA = \frac{EA}{M_t} \quad (1)$$

where M_t is the total mass of the empty beam and the aluminum foam. EA denotes the absorbed energy during the plastic deformation which is calculated as

$$EA = \int_0^{\delta_{max}} f(\delta) d\delta \quad (2)$$

where δ_{max} is the route of the rigid punch, which is equal to 100 mm for all numerical analysis. $f(\delta)$ is the instantaneous crushing force.

F_{ip} and F_m are also designated to be important criterions to evaluate the pedestrian injury in pedestrian-vehicle accidents. F_m denotes the level of average crushing force as calculated by

$$F_m = \frac{EA}{\delta_{max}} \quad (3)$$

F_{ip} and F_m are closely related to the pedestrian and occupant protection in vehicle accidents.

Moreover, to ensure sufficient occupants' survival space, the bending moment M_b was defined to evaluate the bending resistance, which can be calculated as:

$$M_b = (F \times S / 2) / 2 \quad (4)$$

where S denotes the span between the two supports.

2.2 Finite element modeling

It is assumed that the dynamic simulation is conducted by a rigid punch to establish the realistic crash behaviors of the bumper. Figure 1 illustrates the geometric configuration of foam filled under lateral dynamic bending. The upper hat, made of aluminum alloy was installed on the steel lower hat with 48 steel rivets. The specimen has a length of 500 mm and the side length of the cross section is considered as $D = 80$ mm. The heights of upper and lower hats remain unchanged at $h_u = 20$ mm and $h_l = 60$ mm, respectively. The thickness of both hats were kept constants as 1.5 mm. The flange has a width of 20 mm, and the steel rivets with the diameter of 5.2 mm were located by the pitch of 20 mm. The foam-filled beam has an aluminum foam filler with uniform density ρ . The impactor is defined as a moving 35 mm-diameter-cylindrical punch at a constant velocity of 10 m/s. The foam filled profiles lay on two rigid 30 mm-diameter-cylindrical supports with 400 mm span. For the three-bending crash cases, three load positons were examined, including the middle of the span (the first position, P_1), offsetting from the middle spot with 50 mm (the second position, P_2) and a quarter of the span (the third position, P_3), respectively.

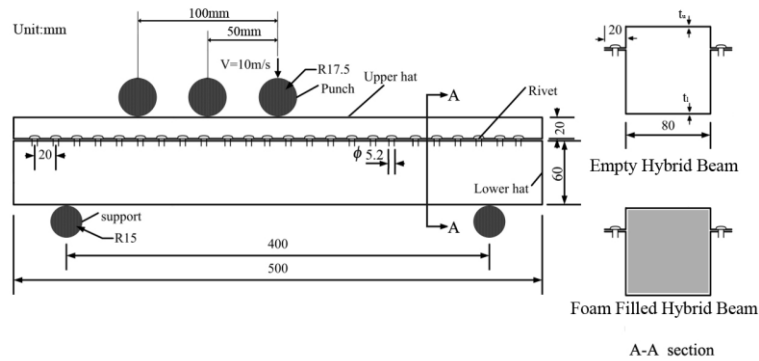


Figure 1. Schematic of foam-filled beams with dissimilar materials for lateral impact.

The representative FE model of foam filled beam is depicted in Figure 2. All the thin-walled hats (the upper hat and the lower hat) were modelled by the Belytschko-Tsay four-node shell elements with 5 integration points through the thickness while one integration point in the element plane. The aluminum foam-filler, the rivets, the cylindrical rigid body were meshed by utilizing eight-node solid elements in LS-DYNA library with reduced integration techniques. Hourglass control was taken into consideration to avoid zero energy deformation modes. The element size of center portion of the beam wall was finer than the rest part on account of localized deformation. Previous study showed that element size of about 2mm for the center part and 4mm for the rest of the specimens, as well as the mesh sizes of 4mm for the foam elements in this model were accepted to be suitable for accuracy and efficiency simultaneously. To account for the contact between the skin and the foam filler, as well as between the beam and the punch or the supports, an “Automatic surface-to-surface contact” algorithm was used. An “Automatic single surface contact” was used for the beams in order to prevent the interpenetration during the deformation process. Moreover, the interface between the rivets and the hats was modelled via a “Tied surface to surface contact”. The static and dynamic friction coefficient for all contact algorithms are set to 0.3 and 0.2^[14], respectively.

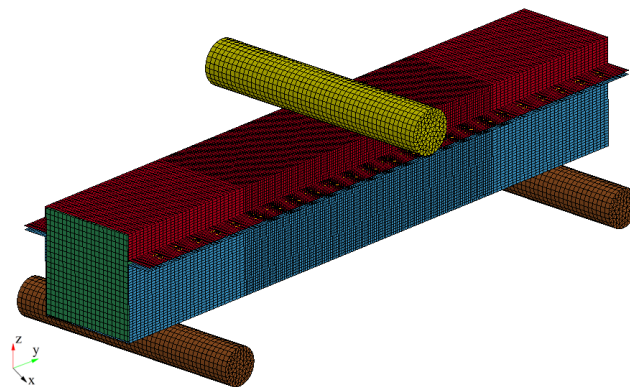


Figure 2. FE model of foam filled beam under lateral impact.

2.2 Material properties

The material models applied herein are the same as that from the Ref^{[15],[16]}. The material properties of AL6063-T6 upper hat and HSS lower hat are tabulated as Table 1. The true stress versus true strain of AL6063-T6 and HSS are illustrated as Figure 3a and Figure 3b. The rivets were modelled of mild steel with the mechanical properties: density $\rho = 7800 \text{ kg/m}^3$, Poisson's ratio $\nu = 0.3$, initial yield stress $\sigma_y = 487.5 \text{ MPa}$ and Young's modulus $E = 200 \text{ GPa}$.

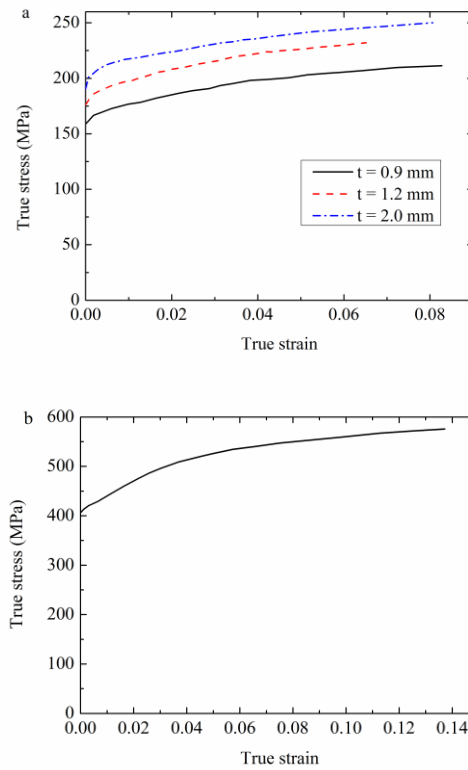


Figure 3. True stress-strain curves of (a) AL6063-T6 [25]; (b) HSS [26].

Table 1 Mechanical properties of hat materials.

| Material | Density ρ_f (kg/m ³) | Young's modulus E (GPa) | Yield stress σ_y (MPa) | Poisson's ratio |
|---------------|--|------------------------------|----------------------------------|-----------------|
| AL6063-T6[15] | 2700 | 64.2 | 162.0 | 0.3 |
| HSS[16] | 7805 | 200.0 | 401.4 | 0.3 |

In the finite element analysis, Mat 24, an elasto-plastic material subject to an arbitrary stress versus strain curve with high strains and high strain rates was applied to predict the behavior of metal materials for the beam. Since the high velocity impact was performed in this study, the strain rate effect of aluminum alloy was neglected as it is strain rate insensitive, while the strain rate effect of steel should be considered. The dynamic yield stress can be obtained by the static strength as followed:

$$\dot{\epsilon} = D \left(\frac{\sigma_{dy}}{\sigma_y} - 1 \right)^n \quad \sigma_{dy} > \sigma_y \quad (5)$$

$$\sigma_{dy} = \sigma_y \left[1 + |\dot{\epsilon} / D|^{1/n} \right]$$

where $\dot{\epsilon}$ is the true strain rate; σ_{dy} denotes the dynamic yield stress on the corresponding strain rate; σ_y is the static yield stress; D and n represent the material constants of steel. It was demonstrated that the predicted results and experimental data meet well when $D = 40 \text{ s}^{-1}$ and $n = 5$. Based on the fact that no failure occurred in the course of verification tests, the material model of rivets was performed by the Mat 100 without failure.

Foam filler was subjected to compressive loads as the high energy absorption capability. The plateau stress, σ_p of aluminum foam is critical for energy absorption, and can be calculated as [15]:

$$\sigma_p = C_{pow} \left(\frac{\rho_f}{\rho_0} \right)^n \quad (6)$$

where ρ_f is aluminum foam density; ρ_0 is the density of foam base material, which is 2700 kg/m³. C_{pow} and n are material constants, which are defined as $C_{pow} = 526$ and $n = 2.17$ according to the uniaxial compressive tests.

Mat 63 is proved to give an accurate performance of foam crashworthiness and have the highest computational efficiency. The foam has a Young's modulus $E = 64.8$ GPa, tensile stress cutoff value of 1.11 and rate sensitivity damping coefficient of 0.05. The Poisson's ratio is 0.01 with no lateral expansion in deformation. Based on the experimental tests proposed by Reyes et al. [17], Hou et al. [18] summarized a simplified stress-strain relationship, as listed in Table 2, to predict the compression behavior of aluminum foam.

Table 2 Stress-strain relationship for aluminum foam.

| | | | | | | |
|--------|---|-------|-----|----------|---------|---------|
| Strain | 0 | p/E | 0.6 | 0.7 | 0.75 | 0.8 |
| Stress | 0 | p | p | $1.35 p$ | $5.0 p$ | $0.05E$ |

3 Results and discussions

3.1 Experimental validation

The validation of FE models were presented in two ways. Firstly, the dynamic bending performance of aluminum-steel double-hats beam with the experiment [13] to verify the accuracy of FE modelling method of riveted empty beam under bending. Secondly, foam material modelling and lateral load behavior were simulated [19].

For the empty beams, the comparative results performed between the experiment and simulation is depicted as Figure 4 (a). The beam made of AL 5052 and SUS304 was subjected to an initial impact loading by a 70 kg rigid cylindered mass in the radius of 65 mm. The initial velocity is 5 m/s. It is observed that a reasonable agreement between the experimental profiles and the present FE model. More detailed comparison of F_{ip} and Mb results from the FE simulations with those from literature for the lateral loads is tabulated as Table 3, and the relative errors of F_{ip} and Mb are obtained as 5.63% and 6.33%, respectively. As plotted in Figure 4 (b), the FE predictions' final deformation and plastic hinges modes are found to meet the requirement for the credibility of the experimental results.

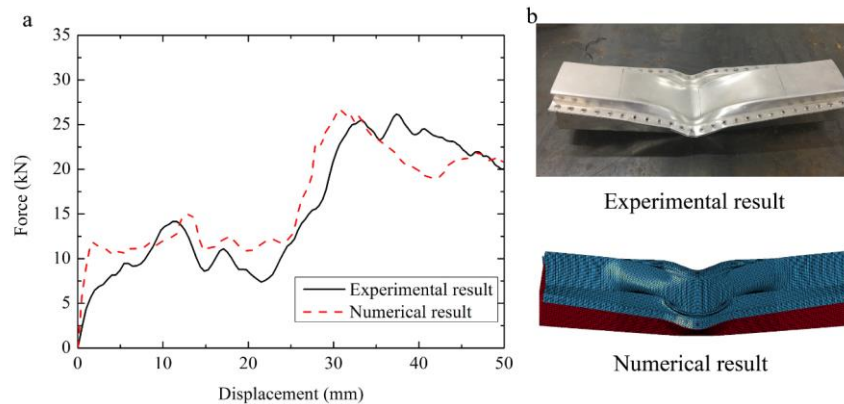


Figure 4. Experimental and Numerical results of dynamic bending for empty hybrid beams: (a) force-displacement curve and (b) final deformation pattern.

Table 3 FE model validation assessment for empty beams [13] and square foam filled columns [19] under lateral loads.

| Test type | F_{ip} (kN) | | | SEA (kJ/kg) | | | Mb (kN*m) | | |
|-------------------|---------------|------|-------|-------------|------|-------|-------------|------|-------|
| | E | N | Re(%) | E | N | Re(%) | E | N | Re(%) |
| Empty hybrid beam | 14.2 | 15.0 | 5.63 | 0.48 | 0.51 | 5.87 | 0.79 | 0.84 | 6.33 |

| | | | | | | | | | |
|---------------------------|------|------|------|---|---|---|------|------|------|
| Square foam filled column | 16.8 | 18.2 | 8.33 | — | — | — | 0.70 | 0.66 | 5.31 |
|---------------------------|------|------|------|---|---|---|------|------|------|

Secondly, to validate the bending conditions of aluminum foam, the crush behaviors of aluminum foam-filled square thin-walled aluminum tubes in aluminum alloy 6060 (AlMgSi0.5F22) were simulated (Figure 5). The deformation mode are also well described by the simulations. The comparison between the experimental and numerical profiles of crashworthiness indices are presented in Table 3. The relative errors of F_{ip} , Mb are blow 10%, which are in agreement with the experiment data.

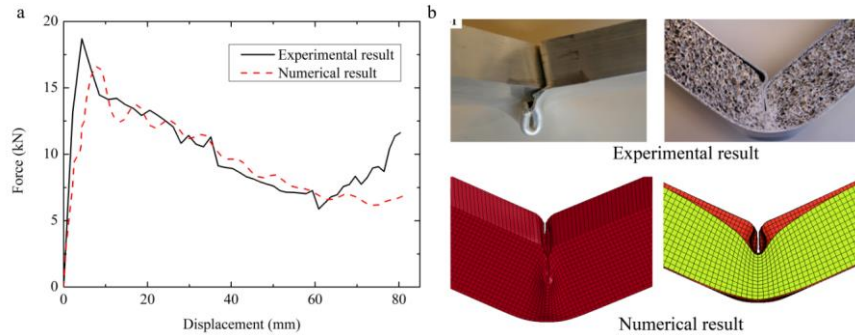


Figure 5. Experimental and Numerical results of dynamic bending for square foam filled column: (a) force-displacement curve and (b) final deformation pattern.

The above-mentioned accuracy validations used in the present work provide sufficient confidence in conducting FEA and multi-optimization of the foam-filled beams with dissimilar materials.

3.2 MDO on specific load position

In this section, the foam-filled beams are optimized for improving the crashworthiness and lightweight under three specific load positions, respectively. The yield stress of the aluminum hat and the foam filler density were set as design variables. For further crashworthiness design and lightweight optimization, F_{ip} and SEA were selected as the optimal objectives for each position.

The MOD problem of foam filled beams under specific position P_i can be formulated as:

$$\begin{cases} \min & F_{ip}^{P_i}(\sigma_y, \rho_f), -SEA^{P_i}(\sigma_y, \rho_f) \\ s.t. & 130MPa \leq \sigma_y \leq 240MPa \\ & 180kg/m^3 \leq \rho_f \leq 360kg/m^3 \end{cases} \quad (7)$$

To form the Pareto Fronts of foam filled beams on specific load position defined as Eq. (7), the MOPSO algorithm was applied in this section based on the corresponding RBF models. A population of 100 design points were generated with Uniform Latin Hypercube (ULH) DoE method, in which the sampling points can be distributed uniformly over all dimensions. Nevertheless, the validated quality of mathematically metamodel need to provide the necessary accuracy to prevent the failure of MOD results. Five random points were selected in the design domain of foam-filled beams with dissimilar materials subjected to three specific load position considered above (P_1, P_2, P_3).

The R_e results from FEA and RBF models for foam filled beams on three impact positions are presented with detailed geometric parameters in Table 4. The relative errors of RBF approximations are less than 4%. Thus the RBF established here are considered adequate for the following optimization.

Table 4 Accuracy assessment of RBF metamodels for foam filled beam under lateral impacts.

| SEA(kJ/kg) | | | Fip(kN) | | |
|------------|-----|-------|---------|-----|-------|
| FEA | RBF | Re(%) | FEA | RBF | Re(%) |

| | | | | | | | |
|---|----|------|------|------|-------|-------|------|
| 1 | P1 | 1.06 | 1.07 | 0.44 | 26.68 | 26.71 | 0.13 |
| | P2 | 1.08 | 1.08 | 0.06 | 26.90 | 26.89 | 0.02 |
| | P3 | 1.27 | 1.27 | 0.15 | 28.46 | 28.45 | 0.03 |
| 2 | P1 | 0.99 | 1.01 | 2.30 | 24.95 | 24.94 | 0.02 |
| | P2 | 1.04 | 1.03 | 0.43 | 25.60 | 25.57 | 0.11 |
| | P3 | 1.28 | 1.27 | 0.51 | 26.54 | 26.59 | 0.20 |
| 3 | P1 | 1.07 | 1.10 | 3.49 | 26.86 | 26.90 | 0.18 |
| | P2 | 1.07 | 1.07 | 0.24 | 27.13 | 27.11 | 0.07 |
| | P3 | 1.27 | 1.28 | 0.75 | 28.50 | 28.53 | 0.12 |
| 4 | P1 | 0.96 | 0.96 | 0.14 | 23.62 | 23.69 | 0.29 |
| | P2 | 1.01 | 1.01 | 0.18 | 24.49 | 24.56 | 0.30 |
| | P3 | 1.27 | 1.27 | 0.36 | 25.63 | 25.69 | 0.22 |
| 5 | P1 | 1.16 | 1.18 | 1.08 | 33.23 | 33.75 | 1.55 |
| | P2 | 1.20 | 1.20 | 0.18 | 33.96 | 33.90 | 0.19 |
| | P3 | 1.47 | 1.47 | 0.01 | 36.59 | 36.74 | 0.42 |

Figure 6 illustrated the conflicted relationship between F_{ip} and SEA on three load positions after iterating for 50 generations. Firstly, in the Pareto plots, the increase in SEA always leads to increase in F_{ip} , vice versa. This justified the efficient application of MOD. The Pareto Fronts of foam filled beam on P3 is located below that on P1 and P2, which also indicates the SEA has a higher value. Moreover, all three Pareto sets distributed in an approximately same scope of F_{ip} .

Secondly, as marked in solid stars in Figure 6, the geometric configurations of foam filled beam and the corresponding crashworthiness indices of ‘ideal optimums’ are summarized in Table 5. There are obvious differences between the optimal configurations for the single objectives on a specific load position: a lower yield stress of aluminum hat and a lower foam filler density lead to a F_{ip} reduction, while higher yield stress and foam density are preferred to SEA maximization. Meanwhile, it is noted that even if the same objective is considered for different load positions, the optimal designs are generally different. For instance, the optimal yield stress to minimize F_{ip} at P1 is 130.0 MPa, while the optimums for the same objective at P2 and P3 are 131.4 MPa and 134.2 MPa, respectively.

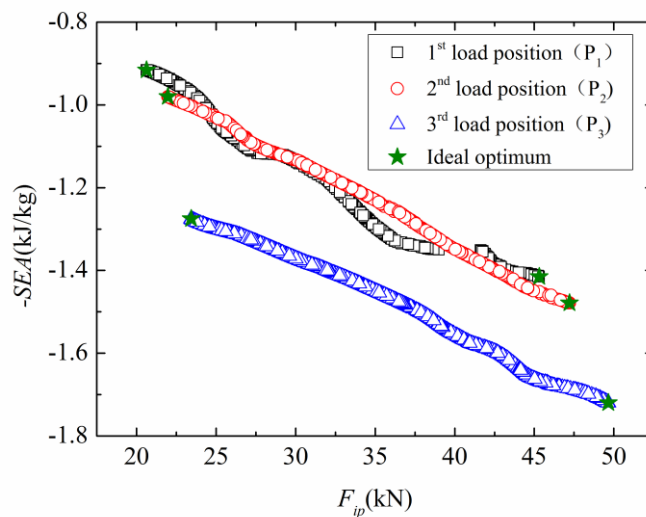


Figure 6. Pareto fronts of F_{ip} vs. SEA on different load position for foam filled beam.

Table 5 Ideal optimums of the two single objective functions for three specific load position.

| Load position | Single objective | σ_y (MPa) | ρ_f (kg/m ³) | SEA (kJ/kg) | | | F_{ip} (kN) | | |
|---------------|------------------|------------------|-------------------------------|---------------|-----|-------|---------------|-----|-------|
| | | | | FEM | RBF | Re(%) | FEM | RBF | Re(%) |

| | | | | | | | | | |
|----|----------------|-------|-----|------|------|------|-------|-------|------|
| P1 | Ideal max. SEA | 236.9 | 360 | 1.44 | 1.42 | 1.39 | 42.12 | 45.31 | 7.57 |
| | Ideal min. Fip | 130.0 | 180 | 0.93 | 0.92 | 1.08 | 19.10 | 20.63 | 8.01 |
| P2 | Ideal max. SEA | 237.4 | 360 | 1.47 | 1.48 | 0.68 | 45.28 | 47.21 | 4.26 |
| | Ideal min. Fip | 131.4 | 180 | 0.97 | 0.98 | 1.03 | 20.24 | 21.97 | 8.55 |
| P3 | Ideal max. SEA | 210.3 | 360 | 1.73 | 1.72 | 0.58 | 51.12 | 49.66 | 2.86 |
| | Ideal min. Fip | 134.1 | 180 | 1.26 | 1.28 | 1.59 | 21.91 | 23.43 | 6.94 |

3.3 MDO on multiple load positions

To deal with load position uncertainty and improve the robust of multiple load positions, a weight-concerned method proposed by Qi et.al^[20], was modified in this section to simplify the design problem and reduce computational cost. In this study, three specific load cases were chosen with a representative positions and a corresponding weight factor. The composite crashworthiness indices (F_{ip}^P , Mb^P and SEA^P) were defined as follows:

$$\begin{aligned}
 F_{ip}^P &= \sum_i^n F_{ip}^{P_i} W^{P_i} \\
 Mb^P &= \sum_i^n Mb^{P_i} W^{P_i} \\
 SEA^P &= \sum_i^n SEA^{P_i} W^{P_i}
 \end{aligned} \tag{8}$$

where the X^{P_i} denotes the structural crashworthiness index on i th load position; n is the total number of impact positions, which is three in this study; W^{P_i} represents the normalized weight factor as:

$$\sum_{i=1}^n W^{P_i} = 1 \tag{9}$$

The workflow of MOD for foam filled beams with load positions variation was shown in Figure 7. Based on this method, the MOD involving multiple load cases can be formulated as:

$$\begin{cases}
 \min & F_{ip}^P(\sigma_y, \rho_f), -SEA^P(\sigma_y, \rho_f), -Mb^P(\sigma_y, \rho_f) \\
 s.t. & 130MPa \leq \sigma_y \leq 240MPa \\
 & 180kg/m^3 \leq \rho_f \leq 360kg/m^3
 \end{cases} \tag{10}$$

To evaluate the effect of weighting factors, two design cases were considered with emphasize on different load positions. The two weighting factors were presented in Table 6. The Design case I assume that P1 is more emphasized, while the Design Case II assume P3 is more emphasized. The RBF models of three crashworthiness indices were constructed for tri-objective optimization.

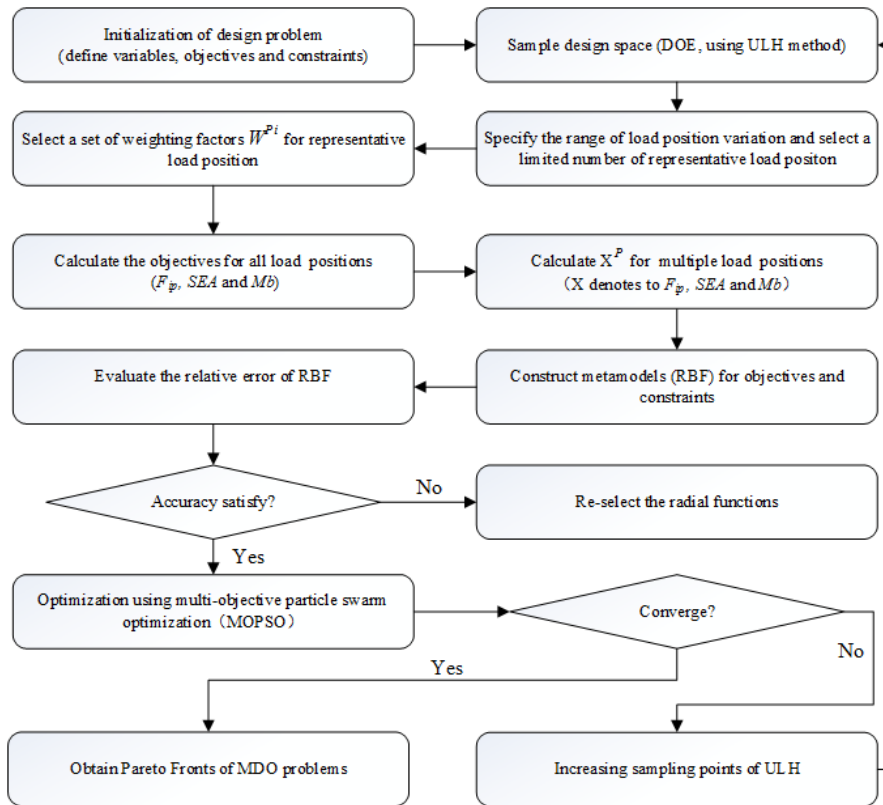


Figure 7. Workflow of multi-objective optimization based on RBF for foam filled beam.

Table 6 Distribution of weighting factors of three specific load positions

| | P1 | P2 | P3 |
|----------------|-----|----|-----|
| Design case I | 0.5 | | 0.2 |
| Design case II | 0.2 | | |

Figure 8 further compares the Pareto fronts of two design cases involving load position uncertainty. The tri-objective Pareto sets were presented in the plane of $-SEA^P - F_{ip}^P$ with Mb^P represented by a color spectrum. It is clearly noted that SEA^P and Mb^P are highly cooperating with each other and both are in confliction against F_{ip}^P , i.e. decrease of F_{ip}^P will reduce SEA^P and Mb^P . The Pareto curves of design case II is closer to the 'utopian point' than that of design case I, which means that SEA of design case II is relatively high, because large weight are assigned to P3 in design case II.

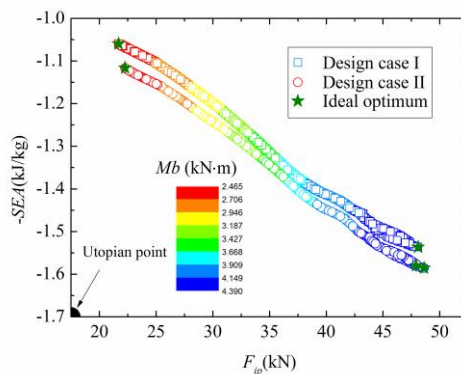


Figure 8. Pareto front of foam-filled beams with dissimilar materials with three objectives.

Table 7 lists the optimal configurations and their crashworthiness performances for a single objective (F_{ip} minimization as well as SEA and Mb maximization), which are marked as solid stars in Figure 8. The optimal yield stress and foam density for SEA^P maximization are fairly different from that for Mb^P maximization. It is noted that weighting factors have some influence on the disproportionate between SEA^P and Mb^P . For instance, in design case I, the yield stress and foam density for SEA maximization were achieved also for Mb maximization. However, in design case II, the yield stress and foam density are 237.0 MPa and 347.9 kg/m³ for Mb maximization, while with SEA maximization considered, the optimal configurations are 209.2 MPa and 355.6 kg/m³.

Table 7 Ideal designs of three single objective functions for foam filled beam under lateral impact.

| | Single objective | σ_y (MPa) | ρ_f (kg/m ³) | SEA (kJ/kg) | F_{ip} (kN) | Mb (kN m) |
|----------------|---------------------|---------------------|----------------------------------|---------------|------------------|-------------|
| Design case I | Ideal max. SEA | 235.8 | 48.09 | 1.54 | 48.09 | 4.39 |
| | Ideal min. F_{ip} | 130.0 | 180.0 | 1.06 | 21.69 | 2.47 |
| | Ideal max. Mb | 235.8 | 48.09 | 1.54 | 47.96 | 4.39 |
| Design case II | Ideal max. SEA | 237.0 | 347.9 | 1.57 | 47.35 | 4.45 |
| | Ideal min. F_{ip} | 145.6 | 192.0 | 1.12 | 23.14 | 2.62 |
| | Ideal max. Mb | 209.2 | 355.6 | 1.57 | 47.42 | 4.48 |

4 Conclusion

In this work, a further study on bending behavior of dissimilar materials thin-walled structure was proposed on the foam filled beams numerically. The foam-filled beams with dissimilar materials had been shown good applications to solve the conflict between F_{ip} and SEA during bumper beam impact. The multi-objective optimization design of foam filled beam with variation in the load positions were formulated to minimize F_{ip} and maximize SEA as well as Mb with respect to yield stress of aluminum hat and foam density. Load positions are proven to be identical for hybrid beams under lateral impact. The multi-objective particle swarm optimization algorithm was applied to generate bi-objective and tri-objective Pareto fronts based on RBF. Pareto fronts were successfully identified for dissimilar materials foam-filled beams' potential on vehicle body.

Acknowledgement

This work is supported by the National Natural Science Foundation of China [grant number 51375066, 51475069, 51475070]; the National Science Foundation of Liaoning Province [grant number 2013020053, 2015021020]; the Fundamental Research Funds for the Central Universities [grant number DUT13LK47, DUT14ZD212].

References

- [1] Min BS, Cho JU. Impact Characteristic According to the Structure of Crash Box at the Vehicle. Archives of Metallurgy and Materials. 62, 2017.
- [2] Patil S, Tay YY, Baratzadeh F, Lankarani H. Modeling of friction-stir butt-welds and its application in automotive bumper impact performance Part 2. Impact modeling and bumper crash performance. Journal of Mechanical Science and Technology. 31:3225-32, 2017.
- [3] Zhang X, Zhang H, Wen Z. Axial crushing of tapered circular tubes with graded thickness. International Journal of Mechanical Sciences. 92:12-23, 2015.
- [4] Zhou Y, Lan F, Chen J. Crashworthiness research on S-shaped front rails made of steel–aluminum hybrid materials. Thin-Walled Structures. 49:291-7, 2011.
- [5] Gedikli H. Crashworthiness optimization of foam-filled tailor-welded tube using coupled finite element and smooth particle hydrodynamics method. Thin-Walled Structures. 67:34-48, 2013.
- [6] Gedikli H. Numerical investigation of axial crushing behavior of a tailor welded tube. Materials & Design. 44:587-95, 2013.
- [7] Meric D, Gedikli H. Energy absorption behavior of tailor-welded tapered tubes under axial impact loading using coupled FEM/SPH method. Thin-Walled Structures. 104:17-33, 2016.
- [8] Wang D-Z, Cao G-J, Qi C, Sun Y, Yang S, Du Y. Crushing Analysis and Lightweight Design of Tapered Tailor Welded Hybrid Material Tubes under Oblique Impact. SAE International Journal of Materials and Manufacturing. 9, 2016.

- [9] Tran T, Hou S, Han X, Chau M. Crushing analysis and numerical optimization of angle element structures under axial impact loading. *Composite Structures*. 119:422-35, 2015.
- [10] Costas M, Díaz J, Romera LE, Hernández S, Tielas A. Static and dynamic axial crushing analysis of car frontal impact hybrid absorbers. *International Journal of Impact Engineering*. 62:166-81, 2013.
- [11] Djamaluddin F, Abdullah S, Ariffin AK, Nopiah ZM. Optimization of foam-filled double circular tubes under axial and oblique impact loading conditions. *Thin-Walled Structures*. 87:1-11, 2015.
- [12] Sun G, Pang T, Zheng G, Song J, Li Q. On energy absorption of functionally graded tubes under transverse loading. *International Journal of Mechanical Sciences*. 115-116:465-80, 2016.
- [13] Qi C, Sun Y, Hu H-T, Wang D-Z, Cao G-J, Yang S. On design of hybrid material double-hat thin-walled beams under lateral impact. *International Journal of Mechanical Sciences*. 118:21-35, 2016.
- [14] Qi C, Yang S. Crashworthiness and lightweight optimisation of thin-walled conical tubes subjected to an oblique impact. *International Journal of Crashworthiness*. 19:334-51, 2014.
- [15] Yang S, Qi C. Multiobjective optimization for empty and foam-filled square columns under oblique impact loading. *International Journal of Impact Engineering*. 54:177-91, 2013.
- [16] Ahmad Z, Thambiratnam DP, Tan ACC. Dynamic energy absorption characteristics of foam-filled conical tubes under oblique impact loading. *International Journal of Impact Engineering*. 37:475-88, 2010.
- [17] Reyes A, Hopperstad OS, Berstad T, Hanssen AG, Langseth M. Constitutive modeling of aluminum foam including fracture and statistical variation of density. *European Journal of Mechanics - A/Solids*. 22:815-35, 2003.
- [18] Hou S, Li Q, Long S, Yang X, Li W. Crashworthiness design for foam filled thin-wall structures. *Materials & Design*. 30:2024-32, 2009.
- [19] Zarei HR, Kröger M. Bending behavior of empty and foam-filled beams: Structural optimization. *International Journal of Impact Engineering*. 35:521-9, 2008.
- [20] Qi C, Yang S, Dong F. Crushing analysis and multiobjective crashworthiness optimization of tapered square tubes under oblique impact loading. *Thin-Walled Structures*. 59:103-19, 2012.